Molecular Vision 2014; 20:56-72 <http://www.molvis.org/molvis/v20/56>
Received 27 August 2013 | Accepted 2 January 2014 | Published 6 January 2014

© 2014 Molecular Vision

Expression profiling of the RPE in zebrafish *smarca4* mutant revealed altered signals that potentially affect RPE and retinal differentiation

Liyun Zhang,[1] Ping Ma,[2] Ross Collery,[3] Sara Trowbridge,[4] Mingzhi Zhang,[5] Wenxuan Zhong,[2] Yuk Fai Leung[1,6]

[1]Department of Biological Sciences, Purdue University, West Lafayette, IN; [2]Department of Statistics, University of Georgia, Athens, GA; [3]Department of Cell Biology, Neurobiology and Anatomy, Medical College of Wisconsin, Milwaukee, WI; [4]Department of Molecular and Cellular Biology, Harvard University, Cambridge, MA; [5]Joint Shantou International Eye Center, Shantou University and the Chinese University of Hong Kong, Shantou, China; [6]Department of Biochemistry and Molecular Biology, Indiana University School of Medicine Lafayette, West Lafayette, IN

Purpose: The purpose of this study was to develop a framework for analyzing retinal pigment epithelium (RPE) expression profiles from zebrafish eye mutants.
Methods: The fish model we used was SWI/SNF-related, matrix associated, actin dependent regulator of chromatin, subfamily a, member 4 (*smarca4*), a retinal dystrophic mutant with a previously described retinal phenotype and expression profiles. Histological and Affymetrix GeneChip analyses were conducted to characterize the RPE defects and underlying differential expression, respectively.
Results: Histological analysis revealed that *smarca4* RPE was formed, but its differentiation was abnormal. In particular, ultrastructural analysis of *smarca4* RPE by transmission electron microscopy demonstrated several defects in melanogenesis. The nature of these defects also suggests that the cytoskeletal dynamics, which are tightly linked with melanogenesis, were impaired in *smarca4* RPE. To compare the expression profile of normal wild-type (WT) and *smarca4* RPE, the gene expression profiles of microdissected retinas and RPE-attached retinas were measured with Affymetrix GeneChip analysis. The RPE expression values were then estimated from these samples by subtracting the retinal expression values from the expression values of the RPE-attached retinas. A factorial analysis was conducted using the expression values of the RPE, retinal, and whole-embryo samples. Specific rules (contrasts) were built using the coefficients of the resulting fitted models to select for three groups of genes: 1) *smarca4*-regulated RPE genes, 2) *smarca4*-regulated retinal genes, and 3) *smarca4*-regulated RPE genes that are not differentially expressed in the retina. Interestingly, the third group consists of 39 genes that are highly related to cytoskeletal dynamics, melanogenesis, and paracrine and intracellular signal transduction.
Conclusions: Our analytical framework provides an experimental approach to identify differentially-regulated genes in the retina and the RPE of zebrafish mutants in which both of these tissues are affected by the underlying mutation. Specifically, we have used the method to identify a group of 39 genes that can potentially explain the melanogenesis defect in the *smarca4* RPE. In addition, several genes in this group are secreted signaling molecules. Thus, this observation further implicates that the *smarca4* RPE might play a role in the retinal dystrophic phenotype in *smarca4*.

The retinal pigment epithelium (RPE) is a single layer of pigmented epithelial cells that supports the function and development of photoreceptors [1]. RPE dysfunction leads to many retinal degenerative diseases, including age-related macular degeneration (AMD) [2] and retinitis pigmentosa (RP) [3,4]. Regeneration [5] and transplantation [6,7] of the RPE could lead to new treatments for these retinal diseases. The success of these therapeutic approaches will rely on our understanding of the genetic regulation of RPE differentiation and paracrine signaling to the retina. A major technical limitation in studying RPE signaling is the difficulty obtaining pure and intact RPE tissue from small developing embryos, which has precluded accurate expression profiling of the RPE during development. We previously addressed this issue by developing an approach for estimating the RPE gene expression profile in the zebrafish by comparing microdissected RPE-attached retinas and RPE-free retinas [8,9]. Subsequently, expression profiling of developing chick [10] and human [11] RPE has been reported. Higdon and colleagues recently demonstrated that RPE-specific gene expression could be detected in purified pigment cells from whole zebrafish embryos, using density gradient centrifugation

Correspondence to: Yuk Fai Leung, Department of Biological Sciences, Purdue University, LILY 2-236, 915 W. State Street, West Lafayette, IN, 47907; Phone: 765-496-3153; FAX: 765-494-0876; email: yfleung@purdue.edu
Dr. Zhang is now at the Department of Ophthalmology, University of Cincinnati, Cincinnati, OH.

and fluorescence-activated cell sorting (FACS) based on the pigment granule density of the cells [12]. The availability of these data sets has substantially facilitated the study of RPE development and the identification of RPE paracrine signals to the retina.

Several paracrine signaling molecules are known to play a role in mediating the interactions between the RPE and the retina during development. For example, pigment epithelium-derived factor (PEDF) is a glycoprotein that has been shown to mediate normal photoreceptor development in the frog [13] and chicken [14]. Two additional signaling molecules, glial cell-derived neurotrophic factor (GDNF) and brain-derived neurotrophic factor (BDNF) are released by cultured human RPE cells, and their presence in culture medium enhances the survival of dopaminergic neurons [15]. Similar to PEDF, GDNF also regulates photoreceptor development in chickens [14,16]. Another class of signaling molecules, Bone morphogenetic protein (Bmp), is also involved in the development of the retina and the RPE. For instance, Bmp4 and Bmp7 expressed in the surface ectoderm overlying the optic vesicle in the chick are essential and sufficient for RPE specification [17]. In addition, Bmp2 and Bmp4 in adult bovine RPE act as potential negative growth regulators and are downregulated during injury in the retina and the RPE [18]. Finally, the canonical wingless (Wnt) signal transduction pathway was recently implicated in RPE development and retinal degeneration. In particular, Wnt activity is essential for transcriptional activation of Mitf and Otx2, two genes that are crucial for RPE specification in mice [19,20]. Interestingly, the conditional knockout of β-catenin in RPE not only affects RPE differentiation but also disrupts retinal morphogenesis and lamination. These findings suggest that Wnt likely mediates signaling interactions between the RPE and the retina.

Although the study of the signaling molecules described above has contributed to our understanding of the interactions between the RPE and the retina, it is clear that only a fraction of the vast genetic network that underlies RPE and retinal development has been described. The purpose of this study was to establish a genomic approach for identifying genes that control RPE differentiation and potential paracrine signals specifically secreted by the RPE. The model we used was a zebrafish SWI/SNF-related, matrix-associated, actin-dependent regulator of chromatin, subfamily a, member 4 (*smarca4*; also known as *yng*) mutant [21]. This mutant has a null mutation in *smarca4,* and was originally described as a model with developmental problems in several organs, including the eye, ear, and heart [22]. *Smarca4* codes for the ATPase of the SWI/SNF chromatin remodeling complex, which is critical to regulation of gene expression during development. As a result of dysregulated gene expression, the retinal structure is disorganized, and appropriate retinal lamination is disrupted in the *smarca4* mutants. The retinal cells are specified but do not fully differentiate. We previously conducted an expression profiling experiment to identify candidate genes that underlie the retinal differentiation phenotype with microarray analysis [23]. The true discovery rate of the study was more than 90% and was highly concordant with the theoretical rate of 95% [24]. Subsequent functional characterizations of the candidate genes have also begun to reveal the gene network regulated by Smarca4 and its role in normal retinal differentiation [25-27].

In addition to the effect on retinal development, the *smarca4* mutation also plays a role in RPE differentiation. In fact, one of the earliest hallmarks used to identify *smarca4* was abnormal RPE pigmentation. We observed the integrity of the RPE layer and its adhesion to the retina were also compromised during our microdissection of *smarca4* retinas [23]. We hypothesized that these defects were caused by abnormal gene expression in *smarca4* RPE. In this study, we first characterized the defects in *smarca4* RPE differentiation with histological analysis. Then, we used our RPE expression analysis approach [8,9] to obtain RPE gene expression in *smarca4*. To identify differential gene expression and potential paracrine signal transduction that might underlie the *smarca4* eye phenotype, an extension of our factorial microarray array analysis [23] was established. In particular, we used the fitted statistical models to build sequential rules (contrasts) to narrow down the list of possible candidate genes.

METHODS

Fish maintenance and embryo collection: The following zebrafish lines were used in this study: wild-type (WT) AB and *smarca4*$^{a50/+}$ (*yng*), which was originally generated from the AB line [21,22]. The WT parents were the genotyped WT siblings of the *smarca4*$^{a50/+}$, and are isogenic other than the *smarca4*^{a50} allele. The adult breeders were maintained according to standard procedures [28]. Embryo collection, staging, and incubation were performed according to standard procedures. The embryos used for an individual experiment were collected from the same parents and spawned within a 15 min interval. All protocols were approved by the Purdue Animal Care and Use Committee.

Microdissection of zebrafish retina and RPE–attached retinas: Microdissection of retinas and RPE-attached retinas from WT and *smarca4* $^{a50/a50}$ embryos at 52 h post-fertilization (hpf) was conducted as described [9]. WT retinas (WR52) and WT RPE-attached retinas (WRR52) were originally

Table 1. The eye tissue samples used in the microarray analysis.

Parameters measured in each replicate (3 replicates per group)	WT retina (WR52)	WT retina+RPE (WRR52)	*smarca4* retina (YR52)	*smarca4* retina+RPE (YRR52)
Number of tissue per replicate	10, 10, 10	10, 10, 10	10, 9, 10	6, 6, 6
RNA yield from extraction (3 replicates)/ ng	170.1, 179.93, 153.22	218.69, 179.83, 266.87	138.6, 164.3, 204.37	112.18, 118.4, 142.1
Input RNA amount for Affymetrix/ ng	33, 33, 33	33, 33, 33	33, 33, 33	24, 24, 24

Four types of eye tissue samples were used in this study, including WT retina (WR52), WT retina+RPE (WRR52), *smarca4* retina (YR52) and *smarca4* retina+RPE (YRR52). Three independent biologic replicates were collected and the number of samples in each replicate is listed. The yield of the total RNAs extracted from these samples and the input RNA amount used for each Affymetrix GeneChip experiment are listed in the Table as well. These parameters were also used in the estimation of RNA expression values as described in Methods.

collected and reported in [8], *smarca4/yng* retinas (YR52) were originally collected and reported in [23], and *smarca4* RPE-attached retinas (YRR52) were collected in this study. Three biologic replicates were collected for each condition, and the number of tissues in each replicate is shown in Table 1.

Total RNA extraction and microarray analysis: Total RNA extraction was performed with an optimized procedure that combined TRIzol (Life Technologies, Grand Island, NY) and column-based purification (Qiagen, Valencia, CA) [8,29]. The yield (Table 1) and the quality of the purified total RNAs were evaluated with NanoDrop spectrophotometry (Thermo Scientific, Wilmington, DE) and Bioanalyzer electrophoresis (Agilent Technologies, Santa Clara, CA), respectively. Total RNAs were amplified and labeled using a two-cycle target-labeling protocol (Affymetrix, Santa Clara, CA), and hybridized to GeneChip Zebrafish Whole Genome arrays (Affymetrix). The input RNA amounts are specified in Table 1. Hybridization, washing, and scanning were performed according to the manufacturer's standard procedure.

Histology: Histological analysis on 1 µm plastic sections was conducted as previously described [8] and imaged with a SPOT-RT3 color slider camera (Diagnostic Instruments, Sterling Heights, MI) mounted on a BX51 fluorescence compound microscope (Olympus, Center Valley, PA). To analyze the ultrastructural changes in the RPE, transmission electron microscopy (TEM) was used. The samples were fixed and processed as previously described [30]. Ultrathin sections (100 nm) through the optic nerve region were collected for TEM analysis with a Philips CM-10 transmission electron microscope (FEI Company, Hillsboro, OR). The resulting images were merged in Adobe Photoshop CS6 (Adobe, San Jose, CA).

In situ hybridization: In situ hybridization was conducted as described [24]. The following riboprobes were used in this study: dopachrome tautomerase (*dct*; GenBank accession number: NM_131555) and retinal pigment epithelium-specific protein 65a (*rpe65a*; NM_200751). To prepare the probes for these genes, a fragment of each gene was amplified from a cDNA library prepared as described [29]. The primer sequences are as follows: dct-1F: 5′-ACT TCT TCG TCT GGC AGC AT-3′, dct-1R: 5′-CGG CTT ATC ATA TCC CTC CA-3′, rpe65–1F: 5′- GCT TCG AGT CGG ATG AAG AG-3′ and rpe65–1R: 5′-CAG GGA CGA AAT GGT TGA GT-3′. The resulting PCR fragment was cloned into the pGEM-T easy vector (Promega, Madison, WI) for propagation. The riboprobes were synthesized according to standard procedures [31].

Morphometric measurements and general statistical analysis: Melanosome and RPE parameters were measured and extracted from the images with i-Solution 10.1 (IMT i-Solution, Burlington, Canada). The morphology of the melanosomes was measured by area and roundness. The latter parameter is defined as $4A/f2\pi$ (A = area, f – max Feret diameter (the longest diameter along the region-of-interest boundary). Thus, 1 = round, 0 = elongated). Standard error propagation was used to combine the measurement errors of the variables. All standard descriptive statistics and data analyses were performed in the R statistical environment version 2.15.2. Melanosome numbers, area and roundness, as well as RPE area were analyzed with standard ANOVA. The melanosomes along the apical/basal axis was demarcated

by the center of the RPE nuclei and their number counted. The resulting data were analyzed with logistic regression. An alpha level of 0.05 was used for all general statistical tests.

Microarray data analysis: The analysis conducted in this study used the WR52, WRR52, YR52, and YRR52 data as described, as well as the whole embryo data obtained from WT (WA52) and *smarca4* (YA52) previously collected [23]. The microarray data were deposited at the Gene Expression Omnibus (GEO) under the accession number (GSE50241).

Probe-level analysis and retinal pigment epithelium expression value estimation: The probe-level data of these sample groups were background-adjusted, normalized, and summarized with a robust multiarray average (RMA) algorithm [32] implemented in the *affy* library of the Bionconductor [33] in R statistical environment version 2.15.2, using default parameters. RPE expression values were estimated from the comparison between the retinal samples and the RPE-attached retinal samples of the same genotype based on a method we previously developed [8]. First, the RMA-normalized expression values in RPE-attached retinal sample were adjusted according to the yield and number of tissues with the following equations:

A. WRR52

$adjExprWRR52_{ij}=ExprWRR52_{ij}$ x

$(mean(yieldWRR52_j/tissueNoWRR52_j)/$

$mean(yieldWR52_j/tissueNoWR52_j))$

B. WR52

$ExprWR52_{ij}$ (i.e., no adjustment)

C. YRR52

$adjExprYRR52_{ij}=ExprYRR52_{ij}$ x

$(mean(yieldYRR52_j/tissueNoYRR52_j)/$

$mean(yieldYR52_j/tissueNoYR52_j))$

D. YR52

$ExprYR52_{ij}$ (i.e., no adjustment)

where Expr is the expression value of a gene i in replicate j, adjExpr is the adjusted expression value of a gene i in replicate j, yield is the total RNA yield of replicate j, and tissueNo is the number of tissue used in replicate j; i=1,…,n; j=1,2,3.

Then, the RPE expression in WT and *smarca4* was estimated as follows:

$RPEWT52=adjExprWRR52_{ij} – ExprWR52_{ij}$

$RPEyng52=adjExprYRR52_{ij} – ExprYR52_{ij}$

Factorial analysis and gene selection: A factorial analysis [23] was conducted using the adjusted RPE expression values, as well as the retinal and whole-embryo values. The overall design is a 3×2 model (Figure 1A) that determines the effect of tissue type (T) and mutation (M) on the expression level. The corresponding levels of each factor are listed below:

Mutation (M) – two levels: WT and smarca4

Tissue (T) – three levels: whole embryo, retina, and RPE

For any gene *g*, its expression (y_g) in the six experimental conditions in Figure 1A was modeled with the following equations:

WT_{embryo}: $y_g = \mu$ (Eq. 2.1)

WT_{retina}: $y_g = \mu + T_R$ (Eq. 2.2)

WT_{RPE}: $y_g = \mu + T_{RPE}$ (Eq. 2.3)

$smarca4_{embryo}$: $y_g = \mu + M$ (Eq. 2.4)

$smarca4_{retina}$: $y_g = \mu + M + T_R + M*T_R$ (Eq. 2.5)

$smarca4_{RPE}$: $y_g = \mu + M + T_{RPE} + M*T_{RPE}$ (Eq. 2.6)

The candidate genes for a specific biologic question were selected by building contrast with the coefficients in Equations 2. In other words, two conditions were statistically compared to identify differentially expressed genes among the conditions (see [23] for further discussion and examples). Depending on whether the two-way interaction term in the Equations 2 was significant or not, the resulting contrasts had to be built differently. In other words, there were first-order (two-way interaction term is not significant) and second-order models (two-way interaction term is significant). Multiple hypothesis testing was corrected by calculating the false discovery rate (FDR). A gene was inferred as differentially expressed when the contrast in consideration had a *q* value less than 0.001 unless specified otherwise. By combining multiple contrasts, specific rules were built to select 1) *smarca4*-regulated RPE genes, 2) *smarca4*-regulated retinal genes, and 3) *smarca4*-regulated RPE genes that are not differentially expressed in the retina (see the corresponding Result sections for the list of contrasts used). A schematic diagram that shows the relationship between these selections and the resulting candidate genes is shown in Figure 1B. General gene annotations were adopted from an annotation file from Affymetrix (Zebrafish annotation release 30). The selected RPE genes were also analyzed with the Database for Annotation, Visualization, and Integrated Discovery (DAVID) v6.7 [34,35] using default parameters. Further grouping was aided by the fold change of a comparison. If an estimated expression value was less than zero, indicating the gene was not expressed in the condition, the value was artificially set as one.

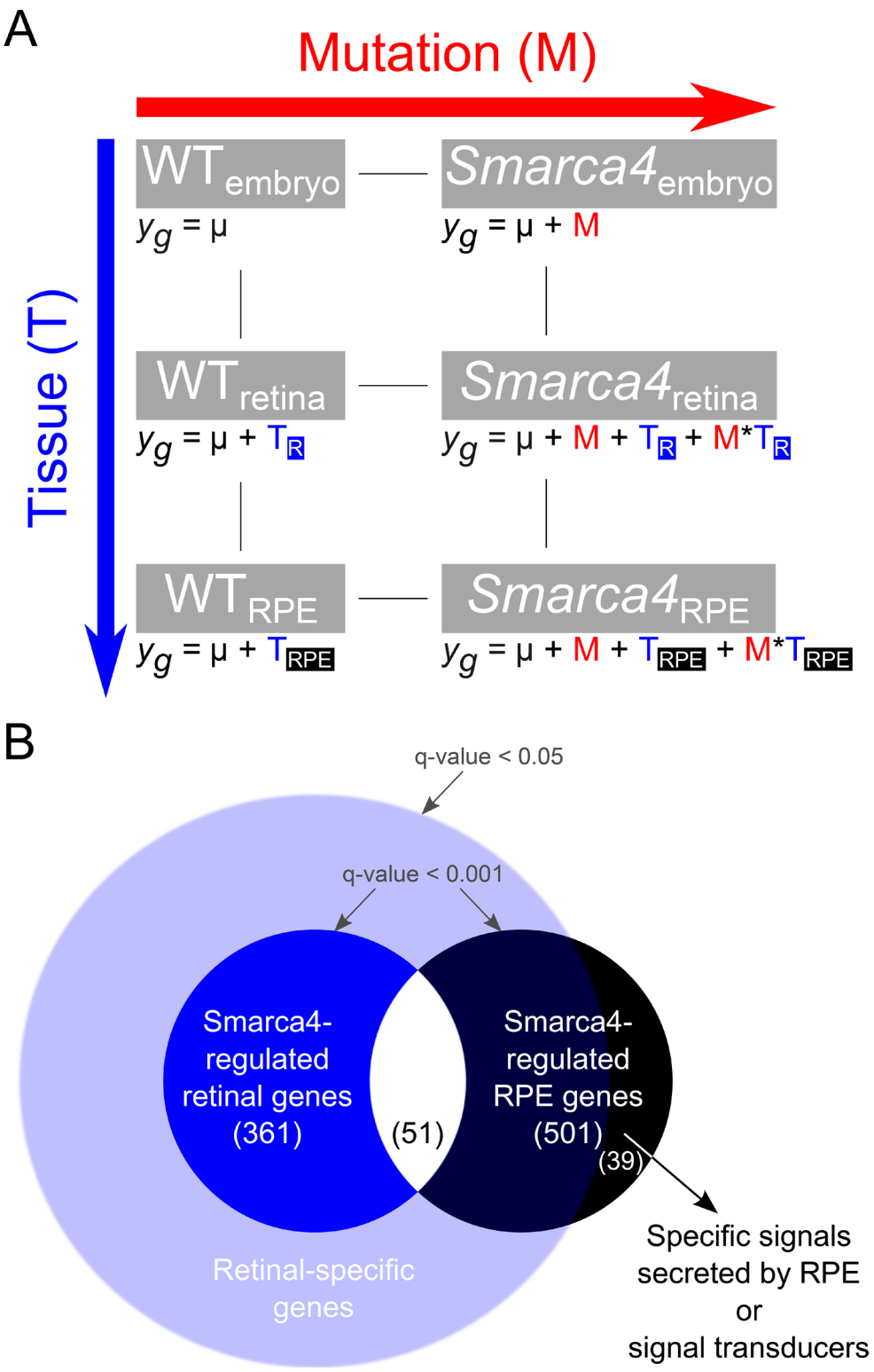

Figure 1. Schematic diagrams of the factorial design and gene selection approach. **A**: A 3x2 factorial design used in the expression data analysis. There are two main factors in the model: Tissue (T) and Mutation (M). The tissue factor T has three levels: whole embryo, retina and RPE, whereas the mutation factor M has two levels: WT and *smarca4*. For each gene *y*, its expression value in different experimental conditions was explained by the corresponding equations. The presence of a factor was represented by a coefficient in the equation. Using the whole family of equations, the statistical modeling explained the contribution of the individual coefficients in the final expression level. **B**: The gene selection was based on statistical testing with the specific combination of the coefficients in the fitted model for a biological question, i.e. contrast. In this study, we further combined several contrasts to develop rules for selecting three groups of genes: i) SWI/SNF related, matrix associated, actin dependent regulator of chromatin, subfamily a, member 4 (*smarca4*)-regulated RPE genes (black circle; Table 3 and Appendix 5), ii) *smarca4*-regulated retinal genes (dark blue circle; Table 4 and Appendix 7), and iii) *smarca4*-regulated RPE genes that are not differentially expressed in the retina (black circle outside the light blue circle; Table 5 and Appendix 9). We theorized that genes that were only differentially expressed in RPE but not retina would constitute two types of genes that may explain the *smarca4* RPE and retinal phenotype. The first type contains signal transducers inside RPE that their dysfunction would cause the *smarca4* RPE defects, while the second type contains signaling molecules that were secreted by RPE that might cause the *smarca4* retinal phenotype. To select this third group of genes, we first obtained a very inclusive group of retinal gene that was differentially expressed in retina (light blue circle). Then, we excluded these genes from the *smarca4*-regulated RPE genes (black circle). Finally, 39 differentially-expressed RPE genes were selected.

RESULTS

Differentiation of smarca4 RPE is abnormal: One distinctive feature of *smarca4* mutant was the lower level of pigmentation in pigment cells, including the RPE. The *smarca4* RPE cells developed pigmentation at around 24 hpf, a stage when the WT RPE cells began to differentiate and form pigment. However, the pigmentation level was always less intense in *smarca4*. By 52 hpf, the whole eye was covered with RPE and appeared dark in the WT (Figure 2A,E), while the *smarca4* RPE cells were noticeably less pigmented, particularly on the ventral side (Figure 2B,F, red arrow). At this stage, there is differentiation of several retinal cell types in the WT eye, and retinal lamination is present [30,36,37]. In contrast, the *smarca4* retina at 52 hpf was dystrophic and would gradually decrease [21-23] (Figure 2F). As a result, the *smarca4* eyes were noticeably different from the WT eyes at 72 hpf (Figure 2C,D,G,H). Although the *smarca4* RPE was more pigmented at this stage, the RPE cells were still abnormal with holes detected in the RPE layer (Figure 2G,H, red arrow).

To analyze the differentiation problem of the *smarca4* RPE, we first conducted an in situ hybridization analysis at 52 hpf with *dct* and *rpe65a*, a pigment cell and an RPE-specific marker, respectively. Dct is a key enzyme in the melanogenesis pathway melanin synthesis [38], which gives the pigment cells the distinctive black color. The *dct* signal generally covered the eye surface of the WT (Figure 2I,K) and *smarca4* embryos (Figure 2J,L), suggesting that the *smarca4* RPE cells were still committed to the pigment cell lineage. However, the *smarca4* staining was irregular, which indicates abnormal RPE differentiation. Indeed, this was supported by the staining of *rpe65a,* an RPE-specific enzyme that mediates a critical step of isomerization of all-trans-retinol to 11-cis-retinal in the visual cycle [39]. In WT embryos, the staining was intense in the anterior region of the eye and highlighted the RPE cell shape clearly (Figure 2M,O), while in the *smarca4* embryos, the staining was irregular (Figure 2N,P), and the extent of staining was far less comprehensive than that observed with *dct* expression (Figure 2J,O).

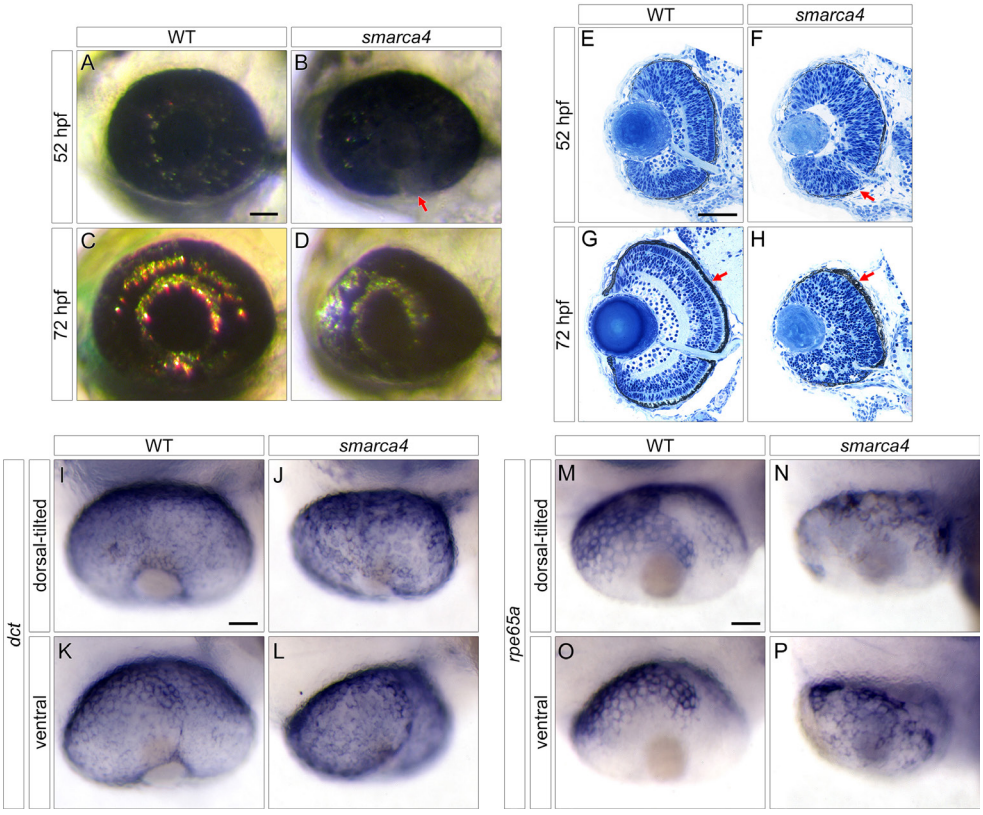

Figure 2. *Smarca4* RPE development is abnormal. **A**–**D**: Whole-mount wild type (WT) and SWI/SNF-related, matrix associated, actin dependent regulator of chromatin, subfamily a, member 4 (*smarca4*) eyes at 52 and 72 h post-fertilization (hpf) are shown. The lateral view is shown. Anterior is to the left, and dorsal is up. The red arrow in **B** indicates a ventral region of *smarca4* where the retinal pigment epithelium (RPE) pigmentation level was lower than the other regions. **E**–**H**: Transverse histological sections of the WT and *smarca4* eyes at 52 and 72 hpf are shown. One distinctive hallmark of *smarca4* is the disruption of their retinal lamination. In addition, the *smarca4* RPE appears paler (**B** and **E**, red arrow) and dysmorphic (**H**, red arrow) compared with the WT. In these sections, lateral is to the left, and dorsal is up. The RPE differentiation problem was further illustrated with in situ hybridization with *dct* (**I**–**L**) and *rpe65a* (**M**–**P**) at 52 hpf. The expression of dct was comparable between WT and *smarca4* RPE, suggesting that the RPE cells in *smarca4* were still committed to the pigment cell lineage. Nonetheless, the differentiation of *smarca4* was abnormal. This was demonstrated by the slightly irregular staining of *dct* and very irregular staining of *rpe65a*, a differentiation marker. In both cases, the dorsal-tilted view (**I**, **J**, **M**, and **N**) and the ventral view (**K**, **L**, **O**, and **P**) are shown, and the anterior side is to the left. Scale bars=50 µm.

The differentiation defects of the *smarca4* RPE were further analyzed with TEM at 52 hpf. The *smarca4* RPE had fewer melanosomes compared with WT (Figure 3A), which is consistent with the pigmentation defects observed in the semithin sections (Figure 2F,H). In addition, there appeared to be fewer melanosomes on the basal side of the cell (red arrow). To quantify these changes, three independent transverse sections of WT and *smarca4* eyes were collected and several RPE attributes measured. First, the number of melanosomes per RPE cell area was analyzed (Figure 3B and Table 2). The RPE on the dorsal and ventral sides of the optic nerve (ON) was analyzed separately. A two-way ANOVA indicated that there were fewer melanosomes/RPE cell area in *smarca4* (p value=1.43e-4) and in the RPE ventral to the ON in both genotypes (p value=4.91e-4; see detailed descriptions of the ANOVA output in Appendix 1). In addition, the total RPE area in the *smarca4* embryos was not smaller than that in the WT embryos (WT: 1176.36±58.24 μm^{-2}; *smarca4*:1078.35±133.05 μm^{-2}; Mann–Whitney test; p value=0.7). Together, these results suggest that there was a general decrease in the melanosome number at this stage. Second, the distribution of the melanosomes in the RPE was evaluated by calculating the apical/basal ratio, using the center of the flattened nuclei to demarcate the apical and basal sides of the RPE cells (Figure 3C and Table 2). A logistic regression analysis of the counts demonstrates that the melanosomes in the *smarca4* RPE had an apical bias (p value=3.47e-12) and that there was a general apical bias in the ventral RPE compared with the dorsal RPE in both genotypes (p value=6.15e-07; Appendix 2).

Melanosomes mature through distinctive phases from the circular immature type to the ellipsoidal mature type [40]. To assess the maturity of the melanosomes, their roundness (1: circular; 0: elongated; Figure 3D and Table 2) and area (Figure 3E and Table 2) were separately evaluated with two-way ANOVA. The analysis shows that the roundness of the melanosomes was not affected by genotype (p value=0.67; Appendix 3). There was also no difference in melanosome roundness between the dorsal and ventral RPE (p value=0.07). These observations suggest that the melanosome maturity, as assessed by shape, was similar between the *smarca4* and WT genotypes. However, there was a small but statistically significant decrease in the melanosome area in *smarca4* RPE (p value=1.96e-7), and in the ventral RPE for both genotypes (p value=2.37e-6; Appendix 4). In addition, the decrease in melanosome size in *smarca4* RPE was less drastic in the ventral side (p value=0.0066). Together, these histological data suggest that *smarca4* RPE cells were formed, but the differentiation was abnormal at 52 hpf. This observation is consistent with the overall impairment of melanogenesis observed in the *smarca4* mutants.

Microarray analysis of smarca4 retina and RPE: The differentiation defects in the smarca4 RPE suggest that the absence of *smarca4* disrupted the regulation and expression of genes that were key to normal RPE differentiation. Furthermore, terminal differentiation was also impaired in the *smarca4* retina, resulting in abnormal retinal lamination (Figure 2F) [21-23]. Since the RPE and the retina interact closely during development, we were interested in elucidating whether the retinal phenotype might be secondary to disruption of normal signals between the developing RPE and retina. To this end, we extended a factorial analysis framework [23] that was previously used to study *smarca4* retinal differentiation. An overview is described (also see the Methods section for the details of the statistical framework).

First, the RPE expression values were estimated by comparing the retinas and the RPE-attached retinas [8]. Then, a 3×2 factorial design (Figure 1A) was used to analyze the expression values of three kinds of tissue (T: whole embryo, retina, and RPE) in two mutation backgrounds (M: WT and *smarca4*). The expression value of a gene in the individual conditions (y_g) was deconstructed into coefficients that represented the contribution to the expression level by the presence of that factor (Figure 1A, equations under the condition name). Using these coefficients, contrasts were built to identify candidate genes that fulfilled specific criteria. The false discovery rate (FDR) q value cutoff for a contrast was 0.001. Several contrasts were ultimately combined to select genes that were regulated by *smarca4* in the retina and the RPE (Figure 1B) and will be discussed below. In addition, a fold-change between *smarca4* and WT was calculated to aid ranking of the resulting gene list.

Smarca4-regulated RPE genes: The contrasts selected genes that were differentially expressed in the WT or *smarca4* RPE and at the same time were regulated by *smarca4*, either directly or indirectly (Figure 1B, black circle; Table 3). A total of 591 genes were selected (Appendix 5). Among them, 432 and 162 genes were under- and overexpressed in the *smarca4* RPE when compared with the WT RPE, respectively. Seven genes had negative RPE expression value in WT and *smarca4* and were not biologically meaningful. DAVID analysis of these genes revealed two functional annotation groups that were highly enriched (Appendix 6; Benjamini-adjusted p value=2.7e-2). These groups include two gene ontology (GO) terms for cellular components: non-membrane-bounded organelle (32 genes/6.1% of total annotated genes) and intracellular non-membrane-bounded organelle (32 genes/6.1% of total annotated genes). These terms refer to organized

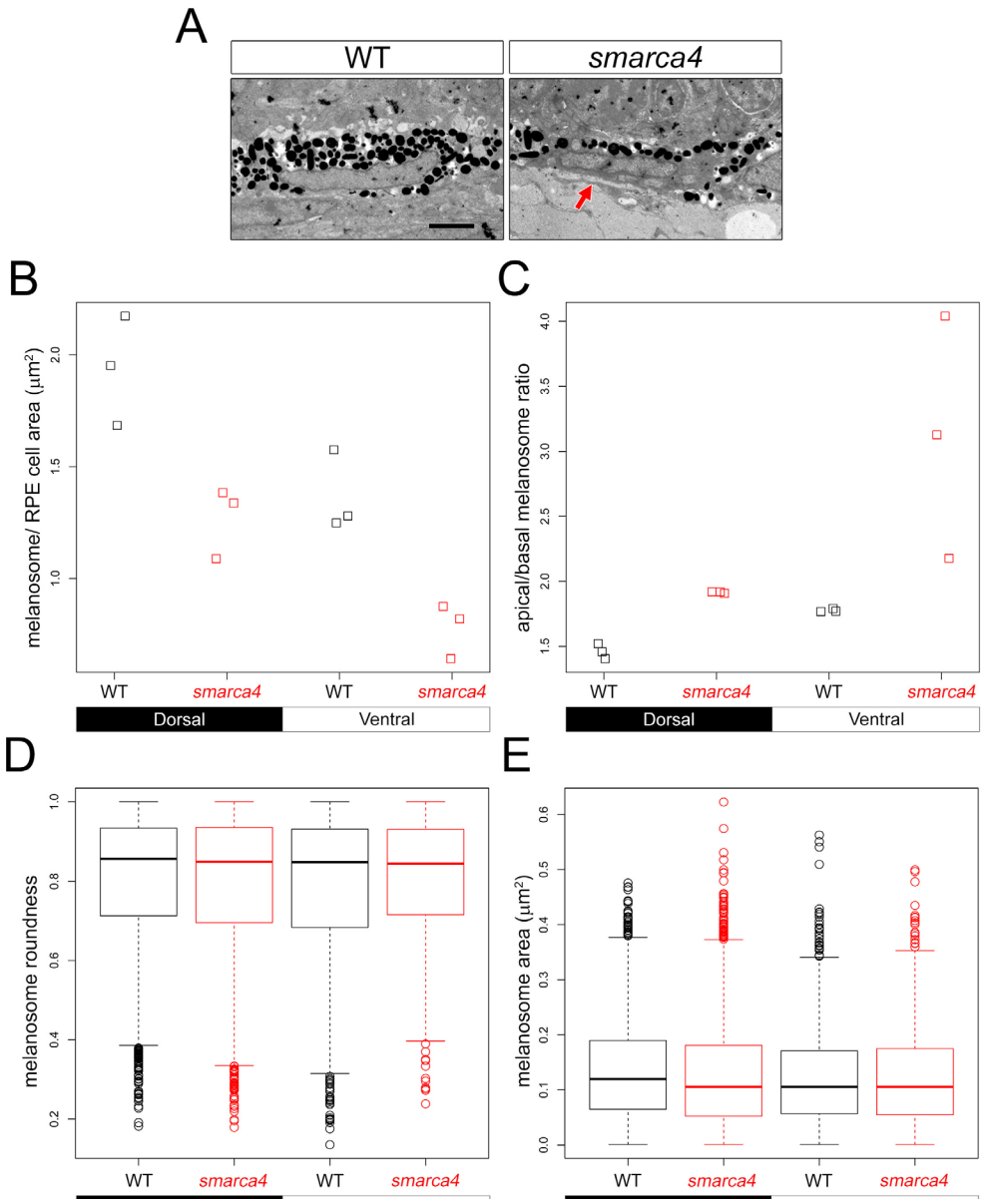

Figure 3. Ultrastructural analysis of *smarca4* RPE with transmission electron microscopy at 52 hpf indicates defects in melanogenesis. **A**: An example retinal pigment epithelium (RPE) cell of wild-type (WT) and *smarca4* is shown. The red arrow indicates the basal side of the RPE cell. Scale bar=5 µm. Three whole-eye transverse sections were collected for each genotype and several morphometric measurements of the melanosomes conducted. The results are shown in **B**–**E**. **B**: A strip chart of the number of melanosome per RPE cell area is shown. **C**: A strip chart of the apical/basal melanosome ratio in the RPE is shown. **D**: A boxplot of the melanosome roundness (1: round; 0: elongated). **E**: A boxplot of the melanosome area. The box plot is a graphical representation based on the distribution of the data. The box shows the interquartile range (IQR) and the thick line inside the box shows the median. The dotted lines show the largest or smallest values that fall within 1.5 times the IQR from the closest edge of the box. Values that are outside this range are considered outliers and were plotted as individual circles. In all these plots, the data obtained from the RPE dorsal and ventral to the optic nerve are plotted separately. The corresponding statistical analyses are shown in Appendix 1–Appendix 4, respectively.

structures that are not bound by a lipid bilayer membrane including the cytoskeleton, suggesting that the cytoskeletal dynamics of the *smarca4* RPE were impaired. Further selection of these RPE candidate genes is described in the third subsection.

Smarca4-regulated retinal genes: The contrasts selected genes that were differentially expressed in the WT or *smarca4* retina and at the same time regulated either directly or indirectly by *smarca4* (Figure 1B, dark blue circle; Table 4). A total of 412 genes were selected (Appendix 7). Among them, 252 and 160 genes were under- and overexpressed in the *smarca4* RPE when compared with the WT RPE, respectively. Many gene candidates were previously identified from a microarray analysis of the *smarca4* retinas [23] and were validated in subsequent follow-up experiments [24,25,27]. Furthermore, we identified the *smarca4* gene itself as underexpressed in the *smarca4* retina, which validated the array experiment and our statistical selection. This is because the null-mutation was expected to result in nonsense-mediated decay of the mRNA and reduce its gene expression. DAVID analysis of these genes revealed several similar

Table 2. Morphometric analyses of melanosomes in WT and *SMARCA4* RPE.

Measurement	WT dorsal RPE (μ±*s*)	WT ventral RPE (μ±*s*)	*smarca4* dorsal RPE (μ±*s*)	*smarca4* ventral RPE (μ±*s*)	Figure and Data analysis
Number of melanosomes/ RPE cell area (μm^{-2})	1.92±0.24	1.36±0.15	1.27±0.14	0.80±0.41	Figure 3B and Appendix 1
Apical/basal ratio	1.46±0.13	1.78±0.18	1.92±0.25	2.77±1.87	Figure 3C and Appendix 2
Roundness (1=round, 0=elongated)	0.81±0.16	0.79±0.18	0.80±0.17	0.80±0.16	Figure 3D and Appendix 3
Area (μm^{-2})	0.14±0.09	0.12±0.09	0.12±0.10	0.13±0.09	Figure 3E and Appendix 4

The four measurements that were analyzed are: number of melanosomes/RPE area, apical/basal ratio, roundness and area. The apical/basal ratio was used to evaluate the distribution of melanosomes inside the RPE cells. The center of the flattened nuclei was used to demarcate the apical and basal side of the RPE cell. Then, the position of the melanosome was scored. The roundness is a measure to evaluate the maturity of the individual melanosomes as the mature ones tend to be ellipsoidal in shape while the immature ones are more circular. Furthermore, the size of the individual melanosome was also evaluated by area measurement. The analysis was also independently done on RPE dorsal and ventral to the optic nerve. The numbers presented are in the format of mean±standard deviation (μ±**s**) . The corresponding plots and data analysis outputs are shown in Figure 3B-D and Appendix 1- Appendix 4 respectively. In summary, there was a reduction in the number of melanosome, an apical bias and a small reduction in area in the *smarca4* RPE. These observations suggest that the melanogenesis was impaired in the *smarca4* RPE.

© 2014 Molecular Vision

Table 3. Contrasts for selecting Smarca4-regulated RPE genes.

Question	Contrast	Number of genes	Appendix
1. Gene differentially expressed in WT RPE	H_0: T_{RPE}=0	6306	-
2. Gene differentially expressed in *smarca4* RPE	H_0: T_{RPE} + M*T_{RPE}=0	4851	-
3. Gene differentially expressed in WT OR *smarca4* RPE	H_0: T_{RPE}=0 OR H_0: T_{RPE} + M*T_{RPE}=0	8536	-
4. Smarca4-regulated RPE genes that are differentially expressed in RPE	H_0: M + M*T_{RPE}=0 AND (H_0: T_{RPE}=0 OR H_0: T_{RPE} + M*T_{RPE}=0)	591	5

These contrasts are listed in the sequential order of building up the final conclusion (Question 4). Each row lists the question, the corresponding contrast that was tested, and the number of genes less than the q-value cutoff (< 0.001). The final 591 selected genes that were selected in Question 4 are listed in Appendix 5. This group of genes is also illustrated in the black circle in Figure 1. These candidate genes are both differentially expressed in the RPE compared with the whole embryo and at the same time regulated by *Smarca4* in the RPE.

functional annotation groups that were enriched (Appendix 8; Benjamini-adjusted p value <0.05; see the table for the gene count and percentage of total annotated genes). For example, eight terms are related to cytoskeletal dynamics, nine terms are related to the cell cycle, and four terms are related to neuron/eye morphogenesis.

Comparing the final list in groups (i) and (ii) showed that 51 genes were commonly expressed in both groups (Figure 1B, the white region between the black and blue circles), while 540 and 361 genes were uniquely expressed in (i) and (ii), respectively. Thus, a total of 952 genes were identified. Among them, 293 (30.78%) had no annotation.

Smarca4-regulated RPE genes that were not differentially expressed in the retina: We theorized that paracrine signaling genes would likely be differentially expressed in one of the two interacting cell-types (i.e., the retina and the RPE), either

Table 4. Contrasts for selecting Smarca4-regulated retinal genes.

Question	Contrast	Number of genes	Appendix
1. Gene differentially expressed in WT retina	H_0: T_R=0	4830	-
2. Gene differentially expressed in *smarca4* retina	H_0: T_R + M*T_R=0	799	-
3. Gene differentially expressed in WT OR *smarca4* retina	H_0: T_R=0 OR H_0: T_R + M*T_R=0	4842	-
4.Smarca4-regulated retinal genes that are differentially expressed in retina	H_0: M + M*T_R=0 AND (H_0: T_R=0 OR H_0: T_R + M*T_R=0)	412	7

These contrasts are listed in the sequential order of building up the final conclusion (Question 4). Each row lists the question, the corresponding contrast that was tested, and the number of genes less than the q-value cutoff (< 0.001). The final 412 selected genes that were selected in Question 4 are listed in Appendix 7. This group of genes is also illustrated in the dark blue circle in Figure 1. These genes are both differentially expressed in the retina compared with the whole embryo and at the same time regulated by Smarca4 in the retina.

Table 5. Contrasts for selecting Smarca4-regulated RPE genes that are not differentially expressed in the retina.

Question	Contrast	Number of genes	Appendix
1. Smarca4-regulated RPE genes that are differentially expressed in RPE	H_0: $M + M*T_{RPE}=0$ AND (H_0: $T_{RPE}=0$ OR H_0: $T_{RPE} + M*T_{RPE}=0$)	591	5
2. Smarca4-regulated RPE genes that are		39	9
i) differentially expressed in RPE, and	i) H_0: $M + M*T_{RPE}=0$ AND (H_0: $T_{RPE}=0$ OR H_0: $T_{RPE} + M*T_{RPE}=0$)		
ii) not differentially expressed in WT retina*, and	NOT		
iii) not differentially expressed in *smarca4* retina*	ii) H_0: $T_R=0$* NOT		
* those genes with a contrast q-value >0.05 will be included	iii) H_0: $T_R + M*T_R=0$* * those genes with a contrast q-value >0.05 will be included		

These contrasts are listed in the sequential order of building up the final conclusion. Each row lists the question, the corresponding contrast that was tested, and the number of genes less than the q-value cutoff (< 0.001; except for *, in which those genes that have a q-value > 0.05 are included. In other words, these genes are also not differentially expressed in the retina. Also see Figure 1). The final 39 selected genes are listed in Appendix 7. In summary, this group of genes is regulated by *Smarca4* and not differentially expressed in the retina. These genes are inside the black circle and outside the light-blue circle in Figure 1.

as secreted ligands or the intracellular signal transducers. To identify these candidate genes in *smarca4* RPE, additional selection criteria were imposed on the group (*i*; Table 5). In particular, these genes should not be differentially expressed in WT or *smarca4* retinas. In other words, we selected for genes with RPE-specific differential expression. Specific contrasts were first built to identify retinal-specific genes in WT and *smarca4* retinas with a relatively inclusive cutoff (*q* value <0.05; Figure 1B, light blue circle). Then, these genes were removed from the candidate gene group (*i*) to select for the genes that were regulated by *smarca4* in the RPE but were not differentially expressed in the retina.

A total of 39 genes were selected based on these criteria (Appendix 9). Among them, 31 were under-expressed in the *smarca4* RPE, while the remaining eight were overexpressed. Based on their annotations and previous investigations in humans [41-44], mice [44-46], chicks [10], and zebrafish [8], we found that many of the known genes are expressed in the RPE and potentially play an important role in RPE signaling and physiology (Appendix 9; supporting evidence columns). For example, previous studies had detected expression of 31 out of 39 (79.5%) genes in the RPE. Among these data, the zebrafish data represent carefully selected RPE genes that were consistently expressed in our previous investigation [8] (Appendix 9). Even if the zebrafish data are excluded from this calculation, studies in the other systems still support the expression of 22 out of 39 (56.4%) genes in RPE. Therefore, these selected *Smarca4*-regulated RPE genes represent a group of highly validated RPE-specific genes. DAVID analysis of these genes also revealed two enriched functional annotation groups with more than two genes in each group (Appendix 10; p value<0.05). These functional annotation groups include the focal adhesion pathway (four genes; 12.5% of total annotated genes) and the melanogenesis pathway (three genes; 9.375% of total annotated genes).

DISCUSSION

This study established an approach for analyzing differential gene expression between the RPE and retina in zebrafish, as well as identifying a group of candidate genes that may underlie the developmental defects observed in the *smarca4* RPE and the retina. Although the analytical emphasis was on the RPE, the same approach could be used to analyze the retina and its secreted signals. This approach focuses on

Table 6. Selected under-expressed Smarca4-regulated RPE genes that were not differentially expressed in the retina revealed potential biologic insights on the morphological defects.

Biological comparison	Potentially relevant biologic functions			
Smarca4*/WT RPE expression fold change	**Cytoskeletal dynamics/ melanosomes formation/ membrane trafficking**	**Secreted/extracellular signals**	**Intracellular signal transducers**	**Other**
<1 (under-expressed in *smarca4* RPE)	*si:ch211–87l2.1, fancl, magi2, map2k1, myl12.2, nav2b, pacrg, pdcl3, ppp1r12a, sec23ip, smarca2, tubb5*	*adam9, bmp8a, gdnf*	*ghdc, guk1a, gsk3b, map2k1, ppp1r12a, spdya, tcf7l1a*	*phyh*

A literature search was conducted on the 39 Smarca4-regulated RPE genes to gain insights into their potential roles in *smarca4* RPE/ retinal development. Several genes that were under-expressed in the *smarca4* RPE have related functional roles in cytoskeletal dynamics, melanogenesis, paracrine and/or intracellular signaling; and the relevance of these functions is elaborated in the discussion section. Some of these genes are listed under different categories as they have multiple functional roles.

tissue-level expression, and thus may complement cell-level approaches, including expression profiling of FACS-purified cells from the RPE-specific reporter lines. An alternative approach to RPE cell purification for expression study is by density gradient centrifugation followed by FACS using pigment granule density as a sorting criterion [12]. This alternative approach may alleviate the need to use RPE-specific reporter lines for RPE expression profiling, which may not be readily applicable to all experimental conditions. However, FACS requires enzymatic dissociation of individual cells, which may affect cell physiology, as well as gene expression. Furthermore, the preparation time from embryos to sorted cells can take several hours. As a result, using FACS for RPE expression analysis may not reveal the desired expression profile at a specific stage. We believe that our approach, which measures at a precise developmental stage, can complement the FACS approach and that together the approaches will facilitate RPE developmental analysis.

Further literature searches revealed potential candidates from the 39 genes in group (iii) that could affect RPE/melanosome differentiation, cytoskeletal dynamics, and cell-cell signaling (Table 6). These observations are also supported by the functional annotation enrichment revealed by the DAVID analysis (Appendix 10). These genes belong to the under-expression category (i.e., *smarca4*/WT RPE expression fold change <1). The first category contains 12 genes (*si:ch211–87l2.1, fancl, magi2, map2k1, myl12.2, nav2b, pacrg, pdcl3, ppp1r12a, sec23ip, smarca2, and tubb5)* that may provide insight into the abnormal RPE development in the *smarca4* mutant, particularly regarding two interdependent processes: cytoskeletal dynamics and melanogenesis [47]. For example, *si:ch211–87l2.1* is a novel gene that is predicted to be a Rab GTPase activator by sequence homology (ZDB-GENE-030131–4497; this is the ID used in the zebrafish community website for the gene). Rab GTPases are small GTPases that regulate membrane trafficking. Functional impairment in specific Rab proteins including Rab32/38 and Rab27A causes pigmentation disorders [48]. Rab27A forms a complex with myosin VIIa and another interacting protein MyRIP, and this complex mediates local trafficking of retinal melanosomes to actin cytoskeleton [49]. Mutations in myosin VIIa in patients with Usher syndrome cause abnormal melanosome distribution in the RPE [50], a phenotype that mimics that seen in the *smarca4* RPE. Together, these observations suggest that the abnormal expression of *si:ch211–87l2.1* might partially underlie the abnormal melanogenesis defects observed in the *smarca4* RPE. Another gene, *fancl*, is an enzyme implicated in Fanconi anemia [51]. One of the clinical symptoms of Fanconi anemia is pigmentation abnormalities [52], which suggests that *fancl* may play also a role in melanogenesis. *Map2k1* is related to melanosome transport (Entrez Gene ID:5604) and pigmentation disorders [52]. *Myl12.2* was identified in a proteomic study of human RPE blebs, abnormal cell membrane structures that may contribute to drusen formation in age-related macular degeneration [41]. *Nav2b* is involved in actin dynamics [53] and plays a role in cell migration and the outgrowth of cellular processes, including axons [54]. *Pacrg* forms a molecular chaperone complex called chaperonin containing TCP1 complex (CCT) [55]. One of its components, CCT4, has been shown to bind to melanosome in a proteomic characterizations [56]. CCT is also involved in the biogenesis of many cytoskeletal proteins, including actins and tubulins. Another selected gene in the category, *Pdcl3/ PhLP2A*, physically interacts with CCT and modulates its folding activity [57]. Thus, the defects in melanogenesis and cytoskeletal dynamics in the *smarca4* RPE might be secondary to dysregulated CCT activity.

Furthermore, *ppp1r12a* (also known as MYPT1 (Entrez Gene ID: 4659)) is a myosin phosphatase. *Smarca2,* another family member of *smarca4,* interacts with the intermediate filament [58](ENSG00000080503). *Magi2* has been shown to be a component of tight junction [59] and is regulated by the planar cell polarity pathway in glomerular podocytes [60]. Together, the under-expression of these genes in *smarca4* RPE might contribute to defects in cytoskeleton and cell-cell adhesion. Consistent with a defect in cell-cell adhesion, we noticed in our experiments that the *smarca4* RPE cells did not adhere to each other well during retinal dissection.

Our statistical design also allowed for the detection of RPE-secreted signals, including *adam9, gdnf*, and *bmp8a,* which may play a role in retinal development and degeneration (Table 6). *Adam9* is a protein secreted by the RPE located within the inter-photoreceptor matrix [61]. *Adam9* is believed to mediate photoreceptor outer segment (POS) attachment to the RPE. *ADAM9* mutations in humans, mice, and dogs cause cone-rod dystrophy [44,62]. In these cases, the apical processes of the RPE are disorganized, and the adhesion between RPE and POS is compromised. We also noticed that the *smarca4* RPE did not tightly adhere to the retina. *Gdnf* is secreted by cultured RPE cells, and its presence in the culture medium enhances the survival of dopaminergic neurons [15]. *Gdnf* also regulates proper photoreceptor development in chickens [14,16]. *Bmp8a*, a member of the Bmp signal transduction pathway, protects mouse osteoblasts from glucocorticoid-induced apoptosis [63]; however, the role of *Bmp8a* in RPE and retinal development has not been fully characterized. The attenuation of secreted signals in the *smarca4* RPE might affect the surrounding tissues, including the retina and the RPE. Furthermore, this observation suggests that other tissues, including paraocular tissues, may play a signaling role in the developmental defects of the *smarca4* retina and RPE, as the *smarca4* mutation affects multiple organ systems.

The third gene category among these 39 selected genes in Table 6 includes intracellular signal transducers that were specifically affected in the RPE and not differentially expressed in the retina. A total of seven genes are in this category, including *ghdc, guk1a, gsk3b, map2k1, ppp1r12a, spdya*, and *tcf7l1a*. These transducers are involved in different cellular processes, and two, *gsk3b* and *tcf7l1a*, are related to Wnt signal transduction. Gsk3β modulates cytoskeletal dynamics [64] and cell-cell adhesion [65] in the RPE, and in turn helps to establish the epithelial phenotype. Tcf7l1a/Tcf3 is a transcriptional repressor and a target of the Wnt signaling pathway [66]. Under the influence of high levels of Wnt signaling, Tcf7l1a degrades and relieves the transcriptional repression on downstream genes [67]. Therefore, under-expression of these genes in *smarca4* RPE implicates over-activation of the Wnt signaling pathway and overexpression of target genes that would normally be repressed. These events might contribute to the abnormal RPE phenotype.

The *phyh* gene was put in a separate gene category in Table 6 because the gene's function as a peroxisomal enzyme does not seem to be directly related to the other genes in our study. Nonetheless, *phyh* mutation in humans causes Refsum disease, and one of the clinical symptoms of this disease is RP [68]. Thus, a decrease *in phyh* in the *smarca4* RPE might also play a role in the *smarca4* phenotype.

The functional annotation analysis of the group (ii) *Smarca4*-regulated retinal genes also revealed enrichment of annotations that are consistent with the *smarca4* retinal phenotype. For example, Link and colleagues showed that there was a cell-cycle withdrawal delay in the *smarca4* retinas [21]. Our analysis identified nine cell-cycle terms enriched in the gene set (Appendix 8). The deregulation of the genes related to these terms in *smarca4* retinas might cause the cell-cycle withdrawal defect. In addition, four and eight terms are related to neuron/retinal differentiation and cytoskeletal dynamics, respectively. This is also consistent with the terminal differentiation defects of the *smarca4* retinas [21,22].

To validate the expression results from this study, quantitative reverse-transcription PCR (qRT-PCR) or northern blot validation should be performed with purified RPE cells rather than estimating the RPE values from dissected eye tissues. This requires generation of RPE reporter lines in WT and *smarca4* for FACS isolation of RPE cells. In Higdon and colleagues' FACS approach, pigment cells were isolated from the whole embryos using pigment granule density [12]. Even though this approach detected an RPE expression signature, it probably requires further optimization before it is applicable to the purification RPE cells from dissected eyes for validation experiments. Laser capture microdissection can be used to obtain some RPE cells but is not feasible for obtaining the whole RPE layer for comparison. Thus, this approach is also not appropriate for validating the findings in this study.

In summary, identifying the *smarca4*-regulated RPE genes with our analysis has highlighted novel and intriguing relationships between RPE cytoskeletal dynamics, membrane trafficking, and intra- and inter-cellular signaling. This new knowledge may ultimately facilitate our understanding of the pathogenesis of related retinal degenerative diseases and development of new therapies.

APPENDIX 1. ANOVA OUTPUT FOR MELANOSOME NUMBER PER RPE CELL AREA ANALYSIS IN FIGURE 3B.

To access the data, click or select the words "Appendix 1."

APPENDIX 2. LOGISTIC REGRESSION OUTPUT FOR MELANOSOMES APICAL-BASAL DISTRIBUTION ANALYSIS IN FIGURE 3C.

To access the data, click or select the words "Appendix 2."

APPENDIX 3. ANOVA OUTPUT FOR MELANOSOME ROUNDNESS ANALYSIS IN FIGURE 3D.

To access the data, click or select the words "Appendix 3."

APPENDIX 4. ANOVA OUTPUT FOR MELANOSOME AREA ANALYSIS IN FIGURE 3E.

To access the data, click or select the words "Appendix 4."

APPENDIX 5. SMARCA4-REGULATED RPE GENES.

To access the data, click or select the words "Appendix 5."

APPENDIX 6. FUNCTIONAL ANNOTATION ENRICHMENT OF SMARCA4-REGULATED RPE GENES.

To access the data, click or select the words "Appendix 6."

APPENDIX 7. SMARCA4-REGULATED RETINAL GENES.

To access the data, click or select the words "Appendix 7."

APPENDIX 8. FUNCTIONAL ANNOTATION ENRICHMENT OF SMARCA4-REGULATED RETINAL GENES.

To access the data, click or select the words "Appendix 8."

APPENDIX 9. SMARCA4-REGULATED RPE GENES THAT ARE NOT DIFFERENTIALLY EXPRESSED IN THE RETINA.

To access the data, click or select the words "Appendix 9."

APPENDIX 10. FUNCTIONAL ANNOTATION ENRICHMENT OF SMARCA4-REGULATED RPE GENES THAT ARE NOT DIFFERENTIALLY EXPRESSED IN THE RETINA.

To access the data, click or select the words "Appendix 10."

ACKNOWLEDGMENTS

We thank Phillip San Miguel and Ann Feil at the Purdue Genomic Core Facility for their excellent assistance on the Affymetrix experiments. We thank Skye Brown and Pin-Chao Liao for their technical assistance. We also thank Brian Link, Woody Walls and members of the Leung laboratory for helpful discussions. This study was partially supported by a Pediatric Ophthalmology Research Grant from the Knights Templar Eye Foundation and a Charles D. Kelman, M.D. Scholar award from the International Retinal Research Foundation to LZ; NSF grants NSF DMS-1222718 to PM and NSF DMS-1120256 to WZ.

REFERENCES

1. Strauss O. The retinal pigment epithelium in visual function. Physiol Rev 2005; 85:845-81. [PMID: 15987797].
2. Lim LS, Mitchell P, Seddon JM, Holz FG, Wong TY. Age-related macular degeneration. Lancet 2012; 379:1728-38. [PMID: 22559899].
3. Daiger SP, Sullivan L, Bowne S. Genes and mutations causing retinitis pigmentosa. Clin Genet 2013; 84:132-41.. [PMID: 23701314].
4. Hartong DT, Berson EL, Dryja TP. Retinitis pigmentosa. Lancet 2006; 368:1795-809. [PMID: 17113430].
5. Karl MO, Reh TA. Regenerative medicine for retinal diseases: activating endogenous repair mechanisms. Trends Mol Med 2010; 16:193-202. [PMID: 20303826].
6. da Cruz L, Chen FK, Ahmado A, Greenwood J, Coffey P. RPE transplantation and its role in retinal disease. Prog Retin Eye Res 2007; 26:598-635. [PMID: 17920328].
7. Carr A-J, Vugler AA, Hikita ST, Lawrence JM, Gias C, Chen LL, Buchholz DE, Ahmado A, Semo M, Smart MJK, Hasan S, da Cruz L, Johnson LV, Clegg DO, Coffey PJ. Protective effects of human iPS-derived retinal pigment epithelium cell transplantation in the retinal dystrophic rat. PLoS ONE 2009; 4:e8152-[PMID: 19997644].
8. Leung YF, Ma P, Dowling JE. Gene expression profiling of zebrafish embryonic retinal pigment epithelium in vivo. Invest Ophthalmol Vis Sci 2007; 48:881-90. [PMID: 17251491].
9. Zhang L, Leung YF. Microdissection of zebrafish embryonic eye tissues. J Vis Exp 2010; xx:2028-[PMID: 20613711].
10. Rizzolo LJ, Chen X, Weitzman M, Sun R, Zhang H. Analysis of the RPE transcriptome reveals dynamic changes during the development of the outer blood-retinal barrier. Mol Vis 2007; 13:1259-73. [PMID: 17679949].
11. Zhang Z, Zhang Y, Xiao H, Liang X, Sun D, Peng S. A gene expression profile of the developing human retinal pigment epithelium. Mol Vis 2012; 18:2961-75. [PMID: 23487591].
12. Higdon CW, Mitra RD, Johnson SL. Gene Expression Analysis of Zebrafish Melanocytes, Iridophores, and Retinal

Pigmented Epithelium Reveals Indicators of Biological Function and Developmental Origin. Leung YF, editor. PLoS One. Public Library of Science; 2013;8:e67801.

13. Jablonski MM, Tombran-Tink J, Mrazek DA, Iannaccone A. Pigment epithelium-derived factor supports normal development of photoreceptor neurons and opsin expression after retinal pigment epithelium removal. J Neurosci 2000; 20:7149-57. [PMID: 11007870].

14. Volpert KN, Tombran-Tink J, Barnstable C, Layer PG. PEDF and GDNF are key regulators of photoreceptor development and retinal neurogenesis in reaggregates from chick embryonic retina. J Ocul Biol Dis Infor. 2009; 2:1-11. [PMID: 20072641].

15. Ming M, Li X, Fan X, Yang D, Li L, Chen S, Gu Q, Le W. Retinal pigment epithelial cells secrete neurotrophic factors and synthesize dopamine: possible contribution to therapeutic effects of RPE cell transplantation in Parkinson's disease. J Transl Med 2009; 7:53-[PMID: 19558709].

16. Rothermel A, Layer PG. GDNF regulates chicken rod photoreceptor development and survival in reaggregated histotypic retinal spheres. Invest Ophthalmol Vis Sci 2003; 44:2221-8. [PMID: 12714664].

17. Müller F, Rohrer H, Vogel-Höpker A. Bone morphogenetic proteins specify the retinal pigment epithelium in the chick embryo. Development 2007; 134:3483-93. [PMID: 17728349].

18. Mathura JR, Jafari N, Chang JT, Hackett SF, Wahlin KJ, Della NG, Okamoto N, Zack DJ, Campochiaro PA. Bone morphogenetic proteins-2 and −4: negative growth regulators in adult retinal pigmented epithelium. Invest Ophthalmol Vis Sci 2000; 41:592-600. [PMID: 10670493].

19. Westenskow P, Piccolo S, Fuhrmann S. Beta-catenin controls differentiation of the retinal pigment epithelium in the mouse optic cup by regulating Mitf and Otx2 expression. Development 2009; 136:2505-10. [PMID: 19553286].

20. Fujimura N, Taketo MM, Mori M, Korinek V, Kozmik Z. Spatial and temporal regulation of Wnt/beta-catenin signaling is essential for development of the retinal pigment epithelium. Dev Biol 2009; 334:31-45. [PMID: 19596317].

21. Link BA, Fadool JM, Malicki J, Dowling JE. The zebrafish young mutation acts non-cell-autonomously to uncouple differentiation from specification for all retinal cells. Development 2000; 127:2177-88. [PMID: 10769241].

22. Gregg RG, Willer GB, Fadool JM, Dowling JE, Link BA. Positional cloning of the young mutation identifies an essential role for the Brahma chromatin remodeling complex in mediating retinal cell differentiation. Proc Natl Acad Sci USA 2003; 100:6535-40. [PMID: 12748389].

23. Leung YF, Ma P, Link BA, Dowling JE. Factorial microarray analysis of zebrafish retinal development. Proc Natl Acad Sci USA 2008; 105:12909-14. [PMID: 18753621].

24. Hensley MR, Emran F, Bonilla S, Zhang L, Zhong W, Grosu P, Dowling JE, Leung YF. Cellular expression of Smarca4 (Brg1)-regulated genes in zebrafish retinas. BMC Dev Biol 2011; 11:45-[PMID: 21756345].

25. Zhang Y, Yang Y, Trujillo C, Zhong W, Leung YF. The expression of irx7 in the inner nuclear layer of zebrafish retina is essential for a proper retinal development and lamination. PLoS ONE 2012; 7:e36145-[PMID: 22540019].

26. Zhang L, Cho J, Ptak D, Leung YF. The role of egr1 in early zebrafish retinogenesis. PLoS ONE 2013; 8:e56108-[PMID: 23405257].

27. Zhang Y, Bonilla S, Chong L, Leung YF. Irx7, a Smarca4-regulated gene for retinal differentiation, regulates other genes controlled by Smarca4 in zebrafish retinas. Gene Expr Patterns 2013; 13:177-82. [PMID: 23557786].

28. Westerfield M. The zebrafish book : a guide for the laboratory use of zebrafish (Danio rerio). 4th ed. Eugene, OR: University of Oregon Press; 2000.

29. Leung YF, Dowling JE. Gene Expression Profiling of Zebrafish Embryonic Retina. Zebrafish 2005; 2:269-83. [PMID: 18248185].

30. Schmitt EA, Dowling JE. Early retinal development in the zebrafish, Danio rerio: light and electron microscopic analyses. J Comp Neurol 1999; 404:515-36. [PMID: 9987995].

31. Nusslein-Volhard C, Dahm R. Zebrafish : a practical approach. 1st ed. Oxford; New York: Oxford University Press; 2002.

32. Irizarry RA, Hobbs B, Collin F, Beazer-Barclay YD, Antonellis KJ, Scherf U, Speed TP. Exploration, normalization, and summaries of high density oligonucleotide array probe level data. Biostatistics 2003; 4:249-64. [PMID: 12925520].

33. Gentleman RC, Carey VJ, Bates DM, Bolstad B, Dettling M, Dudoit S, Ellis B, Gautier L, Ge Y, Gentry J, Hornik K, Hothorn T, Huber W, Iacus S, Irizarry R, Leisch F, Li C, Maechler M, Rossini AJ, Sawitzki G, Smith C, Smyth G, Tierney L, Yang JYH, Zhang J. Bioconductor: open software development for computational biology and bioinformatics. Genome Biol 2004; 5:R80-[PMID: 15461798].

34. Huang W, Sherman BT, Lempicki RA. Bioinformatics enrichment tools: paths toward the comprehensive functional analysis of large gene lists. Nucleic Acids Res 2009; 37:1-13. [PMID: 19033363].

35. Huang W, Sherman BT, Lempicki RA. Systematic and integrative analysis of large gene lists using DAVID bioinformatics resources. Nat Protoc 2009; 4:44-57. [PMID: 19131956].

36. Fadool JM, Dowling JE. Zebrafish: a model system for the study of eye genetics. Prog Retin Eye Res 2008; 27:89-110. [PMID: 17962065].

37. Schmitt EA, Dowling JE. Comparison of topographical patterns of ganglion and photoreceptor cell differentiation in the retina of the zebrafish, Danio rerio. J Comp Neurol 1996; 371:222-34. [PMID: 8835728].

38. Braasch I, Schartl M, Volff J-N. Evolution of pigment synthesis pathways by gene and genome duplication in fish. BMC Evol Biol 2007; 7:74-[PMID: 17498288].

39. Jin M, Li S, Moghrabi WN, Sun H, Travis GH. Rpe65 is the retinoid isomerase in bovine retinal pigment epithelium. Cell 2005; 122:449-59. [PMID: 16096063].

40. Daly CMS, Willer J, Gregg R, Gross JM. snow white, a Zebrafish Model of Hermansky-Pudlak Syndrome Type 5. Genetics 2013; 195:481-94. [PMID: 23893484].

41. Alcazar O, Hawkridge AM, Collier TS, Cousins SW, Bhattacharya SK, Muddiman DC, Marin-Castano ME. Proteomics characterization of cell membrane blebs in human retinal pigment epithelium cells. Mol Cell Proteomics 2009; 8:2201-11. [PMID: 19567368].

42. Munoz-Erazo L, Natoli R, Provis JM, Madigan MC, King NJC. Microarray analysis of gene expression in West Nile virus-infected human retinal pigment epithelium. Mol Vis 2012; 18:730-43. [PMID: 22509103].

43. Yamada Y, Tian J, Yang Y, Cutler RG, Wu T, Telljohann RS, Mattson MP, Handa JT. Oxidized low density lipoproteins induce a pathologic response by retinal pigmented epithelial cells. J Neurochem 2008; 105:1187-97. [PMID: 18182060].

44. Parry DA, Toomes C, Bida L, Danciger M, Towns KV, McKibbin M, Jacobson SG, Logan CV, Ali M, Bond J, Chance R, Swendeman S, Daniele LL, Springell K, Adams M, Johnson CA, Booth AP, Jafri H, Rashid Y, Banin E, Strom TM, Farber DB, Sharon D, Blobel CP, Pugh EN, Pierce EA, Inglehearn CF. Loss of the metalloprotease ADAM9 leads to cone-rod dystrophy in humans and retinal degeneration in mice. Am J Hum Genet 2009; 84:683-91. [PMID: 19409519].

45. Cottet S, Michaut L, Boisset G, Schlecht U, Gehring W, Schorderet DF. Biological characterization of gene response in Rpe65−/− mouse model of Leber's congenital amaurosis during progression of the disease. FASEB J 2006; 20:2036-49. [PMID: 17012256].

46. Rattner A, Toulabi L, Williams J, Yu H, Nathans J. The genomic response of the retinal pigment epithelium to light damage and retinal detachment. J Neurosci 2008; 28:9880-9. [PMID: 18815272].

47. Wasmeier C, Hume AN, Bolasco G, Seabra MC. Melanosomes at a glance. J Cell Sci 2008; 121:3995-9. [PMID: 19056669].

48. Ohbayashi N, Fukuda M. Role of Rab family GTPases and their effectors in melanosomal logistics. J Biochem 2012; 151:343-51. [PMID: 22323658].

49. El-Amraoui A, Schonn J-S, Küssel-Andermann P, Blanchard S, Desnos C, Henry J-P, Wolfrum U, Darchen F, Petit C. MyRIP, a novel Rab effector, enables myosin VIIa recruitment to retinal melanosomes. EMBO Rep 2002; 3:463-70. [PMID: 11964381].

50. Liu X, Ondek B, Williams DS. Mutant myosin VIIa causes defective melanosome distribution in the RPE of shaker-1 mice. Nat Genet 1998; 19:117-8. [PMID: 9620764].

51. Kottemann MC, Smogorzewska A. Fanconi anaemia and the repair of Watson and Crick DNA crosslinks. Nature 2013; 493:356-63. [PMID: 23325218].

52. Baxter LL, Pavan WJ. The etiology and molecular genetics of human pigmentation disorders. Wiley Interdiscip Rev Dev Biol. 2013; 2:379-92. [PMID: 23799582].

53. Schmidt KL, Marcus-Gueret N, Adeleye A, Webber J, Baillie D, Stringham EG. The cell migration molecule UNC-53/NAV2 is linked to the ARP2/3 complex by ABI-1. Development 2009; 136:563-74. [PMID: 19168673].

54. Peeters PJ, Baker A, Goris I, Daneels G, Verhasselt P, Luyten WHML, Geysen JJGH, Kass SU, Moechars DWE. Sensory deficits in mice hypomorphic for a mammalian homologue of unc-53. Brain Res Dev Brain Res 2004; 150:89-101. [PMID: 15158073].

55. Imai Y, Soda M, Murakami T, Shoji M, Abe K, Takahashi R. A product of the human gene adjacent to parkin is a component of Lewy bodies and suppresses Pael receptor-induced cell death. J Biol Chem 2003; 278:51901-10. [PMID: 14532270].

56. Chi A, Valencia JC, Hu Z-Z, Watabe H, Yamaguchi H, Mangini NJ, Huang H, Canfield VA, Cheng KC, Yang F, Abe R, Yamagishi S, Shabanowitz J, Hearing VJ, Wu C, Appella E, Hunt DF. Proteomic and bioinformatic characterization of the biogenesis and function of melanosomes. J Proteome Res 2006; 5:3135-44. [PMID: 17081065].

57. Stirling PC, Srayko M, Takhar KS, Pozniakovsky A, Hyman AA, Leroux MR. Functional interaction between phosducin-like protein 2 and cytosolic chaperonin is essential for cytoskeletal protein function and cell cycle progression. Mol Biol Cell 2007; 18:2336-45. [PMID: 17429077].

58. Barbe L, Lundberg E, Oksvold P, Stenius A, Lewin E, Björling E, Asplund A, Pontén F, Brismar H, Uhlén M, Andersson-Svahn H. Toward a confocal subcellular atlas of the human proteome. Mol Cell Proteomics 2008; 7:499-508. [PMID: 18029348].

59. Lehtonen S, Ryan JJ, Kudlicka K, Iino N, Zhou H, Farquhar MG. Cell junction-associated proteins IQGAP1, MAGI-2, CASK, spectrins, and alpha-actinin are components of the nephrin multiprotein complex. Proc Natl Acad Sci USA 2005; 102:9814-9. [PMID: 15994232].

60. Babayeva S, Zilber Y, Torban E. Planar cell polarity pathway regulates actin rearrangement, cell shape, motility, and nephrin distribution in podocytes. Am J Physiol Renal Physiol 2011; 300:F549-60. [PMID: 20534871].

61. den Hollander AI, Black A, Bennett J, Cremers FPM. Lighting a candle in the dark: advances in genetics and gene therapy of recessive retinal dystrophies. J Clin Invest 2010; 120:3042-53. [PMID: 20811160].

62. Goldstein O, Mezey JG, Boyko AR, Gao C, Wang W, Bustamante CD, Anguish LJ, Jordan JA, Pearce-Kelling SE, Aguirre GD, Acland GM. An ADAM9 mutation in canine cone-rod dystrophy 3 establishes homology with human cone-rod dystrophy 9. Mol Vis 2010; 16:1549-69. [PMID: 20806078].

63. Kósa JP, Kis A, Bácsi K, Balla B, Nagy Z, Takács I, Speer G, Lakatos P. The protective role of bone morphogenetic protein-8 in the glucocorticoid-induced apoptosis on bone cells. Bone 2011; 48:1052-7. [PMID: 21277400].

64. Salinas PC. Modulation of the microtubule cytoskeleton: a role for a divergent canonical Wnt pathway. Trends Cell Biol 2007; 17:333-42. [PMID: 17643305].

65. Burke JM. Epithelial phenotype and the RPE: is the answer blowing in the Wnt? Prog Retin Eye Res 2008; 27:579-95. [PMID: 18775790].

66. Wu C-I, Hoffman JA, Shy BR, Ford EM, Fuchs E, Nguyen H, Merrill BJ. Function of Wnt/β-catenin in counteracting Tcf3 repression through the Tcf3-β-catenin interaction. Development 2012; 139:2118-29. [PMID: 22573616].

67. Shy BR, Wu C-I, Khramtsova GF, Zhang JY, Olopade OI, Goss KH, Merrill BJ. Regulation of Tcf7l1 DNA Binding and Protein Stability as Principal Mechanisms of Wnt/β-Catenin Signaling. Cell Rep. 2013; 4:1-9. [PMID: 23810553].

68. Jansen GA, Hogenhout EM, Ferdinandusse S, Waterham HR, Ofman R, Jakobs C, Skjeldal OH, Wanders RJ. Human phytanoyl-CoA hydroxylase: resolution of the gene structure and the molecular basis of Refsum's disease. Hum Mol Genet 2000; 9:1195-200. [PMID: 10767344].

Articles are provided courtesy of Emory University and the Zhongshan Ophthalmic Center, Sun Yat-sen University, P.R. China. The print version of this article was created on 6 January 2014. This reflects all typographical corrections and errata to the article through that date. Details of any changes may be found in the online version of the article.